A single combination gene therapy treats multiple age-related diseases

Noah Davidsohn[a,b], Matthew Pezzone[a], Andyna Vernet[a], Amanda Graveline[a], Daniel Oliver[a], Shimyn Slomovic[a], Sukanya Punthambaker[a,b], Xiaoming Sun[c], Ronglih Liao[d,e], Joseph V. Bonventre[c], and George M. Church[a,b,1]

[a]Wyss Institute for Biologically Inspired Engineering at Harvard University, Boston, MA 02115; [b]Department of Genetics, Harvard Medical School, Boston, MA 02115; [c]Brigham and Women's Hospital, Boston, MA 02115; [d]Division of Genetics, Department of Medicine, Brigham and Women's Hospital, Harvard Medical School, Boston, MA 02115; and [e]Division of Cardiovascular Medicine, Department of Medicine, Brigham and Women's Hospital, Harvard Medical School, Boston, MA 02115

Comorbidity is common as age increases, and currently prescribed treatments often ignore the interconnectedness of the involved age-related diseases. The presence of any one such disease usually increases the risk of having others, and new approaches will be more effective at increasing an individual's health span by taking this systems-level view into account. In this study, we developed gene therapies based on 3 longevity associated genes (fibroblast growth factor 21 [FGF21], αKlotho, soluble form of mouse transforming growth factor-β receptor 2 [sTGFβR2]) delivered using adeno-associated viruses and explored their ability to mitigate 4 age-related diseases: obesity, type II diabetes, heart failure, and renal failure. Individually and combinatorially, we applied these therapies to disease-specific mouse models and found that this set of diverse pathologies could be effectively treated and in some cases, even reversed with a single dose. We observed a 58% increase in heart function in ascending aortic constriction ensuing heart failure, a 38% reduction in α-smooth muscle actin (αSMA) expression, and a 75% reduction in renal medullary atrophy in mice subjected to unilateral ureteral obstruction and a complete reversal of obesity and diabetes phenotypes in mice fed a constant high-fat diet. Crucially, we discovered that a single formulation combining 2 separate therapies into 1 was able to treat all 4 diseases. These results emphasize the promise of gene therapy for treating diverse age-related ailments and demonstrate the potential of combination gene therapy that may improve health span and longevity by addressing multiple diseases at once.

gene therapy | AAV | combination therapy | age-related diseases

Despite the interconnected nature of age-related diseases (1–3), preventing or treating the sum of their diverse pathologies cannot be achieved by modulating a single genetic pathway. Also, while alteration of a single longevity-associated gene using transgenic mice has been shown to improve health span and extend life span by up to 30% (4–6), acting on insight gained from such transgenic or loss-of-function models to generate practical therapies for adult nontransgenic animals has met with little success (7, 8). For instance, there are a number of traditional small molecule therapies that aim to influence longevity gene pathways, yet none are Food and Drug Administration (FDA) approved, and the possibility of related side effects is a concern (9–11). Furthermore, traditional methods by their nature largely ignore the relation between age-related diseases, narrowly influencing a particular pathway involved in the pathogenesis of a single disease. An alternative approach that may relieve the bottleneck between antiaging transgenics and therapeutics is the delivery and direct modulation of longevity gene expression via adeno-associated virus (AAV)-mediated gene therapy (12). Even so, targeting gene therapy to a single pathology cannot correct or prevent the deterioration of health span that results from multiple age-related diseases and not just one.

In this work, we developed and tested 3 AAV-based gene therapies and administered them to adult nontransgenic mice for the treatment of 4 age-related diseases. The 3 genes involved in these therapies were fibroblast growth factor 21 (FGF21), αKlotho, and transforming growth factor-β1 (TGFβ1). These 3 genes were chosen due to their known beneficial role in aging and specific disease states (4–6). FGF21 and αKlotho are circulating factors produced by the liver and kidney, respectively (5, 13–15), and TGFβ1 is a secreted factor with expression that is not limited to a particular organ (16). FGF21 has established roles in metabolism and glucose handling (17), αKlotho is a known regulator of intracellular calcium and provides protection in heart and kidney pathologies (18, 19), and TGFβ1 signaling plays an important role in age-related hypertrophic cardiomyopathy, immune recruitment, and extracellular matrix formation (20). Although these 3 genes have known roles in various age-associated disease states, it remains unknown whether their simultaneous perturbation would provide an additive, synergistic, or deleterious phenotype in any given disease.

Results

We selected AAV as the gene therapy delivery method due to its safety, low immunogenicity, ease of manufacturing, ability to infect

Significance

Human and animal longevity is directly bound to their health span. While previous studies have provided evidence supporting this connection, therapeutic implementation of this knowledge has been limited. Traditionally, diseases are researched and treated individually, which ignores the interconnectedness of age-related conditions, necessitates multiple treatments with unrelated substances, and increases the accumulative risk of side effects. In this study, we address and overcome this deadlock by creating adeno-associated virus (AAV)-based antiaging gene therapies for simultaneous treatment of several age-related diseases. We demonstrate the modular and extensible nature of combination gene therapy by testing therapeutic AAV cocktails that confront multiple diseases in a single treatment. We observed that 1 treatment comprising 2 AAV gene therapies was efficacious against all 4 diseases.

APPLIED BIOLOGICAL SCIENCES

dividing and nondividing cells, and a growing number of successful human clinical trials (21–23). We began by creating 3 separate AAV8 vectors to overexpress mouse FGF21, a soluble form of mouse transforming growth factor-β receptor 2 (sTGFβR2) that binds and represses TGFβ1 (24), and mouse αKlotho (*Methods* and *SI Appendix*, Fig. S1*A*). The AAV8 serotype was chosen as the delivery vector due to its high infection rate of the liver (25), an organ well known for its ability to produce high levels of secreted proteins (26) and the natural tissue for endogenous FGF21 expression (4). Following the generation and injection of each virus, we verified overexpression of the corresponding transgenes directly or from their downstream effect in mouse plasma using enzyme-linked immunosorbent assay (ELISA) and western blots (*Methods* and *SI Appendix*, Fig. S1 *B–D*) and found up to a 17-fold increase in FGF21, a 95% decrease in circulating TGFβ1, and an ~10× increase in circulating αKlotho. We also performed full necropsies on mice injected with our therapies, and no remarkable pathological findings were noted, suggesting no harmful effects compared with control mice.

Obesity afflicts more than 1 in 3 adults of the US population and is responsible for an overall decrease in health and increased risks for cancer, heart disease, and neurological deterioration among many others (27). In light of FGF21's reported role in metabolism and fat homeostasis, we hypothesized that sustained overexpression of FGF21 could counter metabolic dysregulation resulting from a high-fat diet (HFD), which is an established model for obesity and type II diabetes in mice (28). It has also been observed that αKlotho can help regulate high blood glucose in diabetes models (29) and that TGFβ1 signaling and other inflammatory pathways also impact obesity and disease (30–32). Accordingly, we sought to investigate if a synergistic advantage could be achieved through the coexpression of αKlotho, FGF21, and sTGFβR2. Mice were fed an HFD for 3 mo, which yielded an average weight increase of 15 g (56%) per mouse compared with mice fed a normal diet (ND) (*Methods*). Of note, the mice were maintained on an HFD throughout the experiment (pre- and postinjection) to accurately reflect the reticent nature of human dietary habits. HFD mice were infected with AAV:FGF21 (F), AAV:sTGFβR2 (T), and AAV:αKlotho (K) individually or in combination (Fig. 1*A*). An AAV:GFP (C) vector was used in the control groups. Recipients of the AAV:FGF21 therapy, regardless of any other treatment, experienced a complete reversal of the obese phenotype within 40 d postinjection that was maintained throughout the study (3 mo), despite the continued HFD (Fig. 1 *B* and *C*). To further investigate how permanent this phenotype was, we also kept mice that received only the AAV:FGF21 therapy on an HFD for 8 mo and did not observe any weight reversal (Fig. 1*D*). It is unclear whether, at the applied AAV:FGF21 dose, any synergism could possibly be observed given the overwhelming effect of FGF21 alone. A slightly diminished effect from both AAV:sTGFβR2 and AAV:αKlotho in combination with AAV:FGF21 was observed, although not statistically significant.

To evaluate if our therapy could also mitigate age-related obesity, 18-mo-old aged mice on an ad libitum ND were used. These mice tend to naturally experience increased adiposity and weighed on average 40 g. We injected all 3 constructs individually or in combination into these mice, resulting in a return to a lean body weight of 30 g for mice that received AAV:FGF21 alone or in combination within 100 d postinjection, which was maintained until at least the 150-d mark (Fig. 1*E*). Interestingly, we witnessed a decrease in weight in all therapy groups that received AAV:αKlotho as well. AAV:αKlotho alone and in combination with AAV:sTGFβR2 was able to achieve up to 15% weight loss in naturally occurring age-related obesity but did not show any weight loss effects in middle-aged mice fed an HFD.

To further evaluate the effect of AAV:FGF21 on mice fed an HFD, the animals were placed in metabolic chambers, and their activity, food intake, O_2 consumption, and CO_2 production were
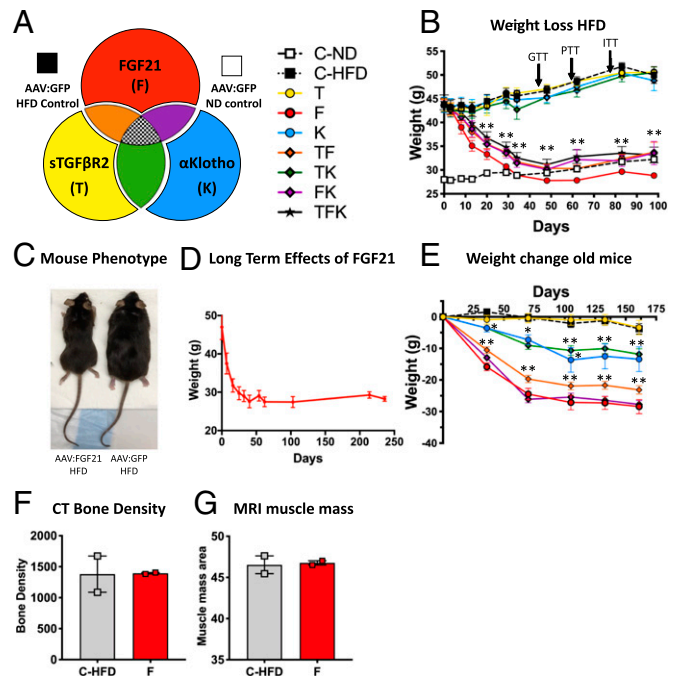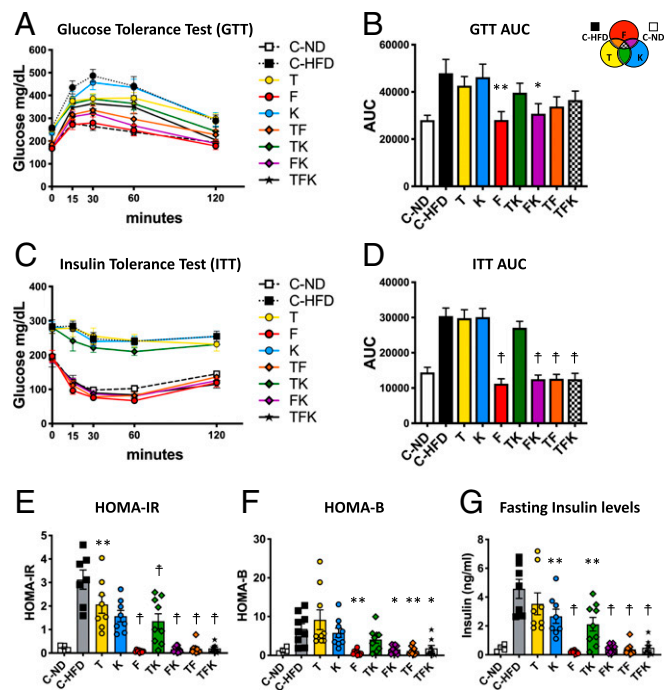

Fig. 1. Systemic AAV delivery of combination gene therapy reverses symptoms of obesity for mice on an HFD. (*A*) Venn diagram of the combinations of gene therapies explored as well as the color coding for all subsequent graphs. FK, FGF21 + αKlotho. (*B*) Weight of mice over time injected with a control vector AAV:GFP on an ND or an HFD, and mice on an HFD injected with individual or all combinations of AAV:FGF21, AAV:sTGFbR2, or AAV:αKlotho. *n* = 10 for AAV:GFP ND mice, and *n* = 12 for AAV:GFP and all therapy-treated HFD mice. (*C*) Phenotype exhibited by mice on an HFD with control vector (*Right*) and AAV:FGF21 vector (*Left*). (*D*) Long-term effect on mice receiving an HFD of the AAV:FGF21 therapy up to 250 d postinjection (*n* = 4). (*E*) Percentage weight change of 18-mo-old mice on an ND with starting weight ~40 g (*n* = 25 for each group). (*F*) CT scan of mice observing bone density after administration of AAV:FGF21 (*n* = 2 for each group). (*G*) Quantified muscle mass of MRI of whole mouse (*n* = 2 for each group). Statistical tests in *B* and *E* are 2-way ANOVA. Statistical tests in *F* and *G* are 2-sided *t* tests. Error bars represent SEM. C, control; F, FGF21; K, αKlotho; T, sTGFβR2; TF, sTGFβR2 + FGF21; TFK, sTGFβR2 + FGF21 + αKlotho; TK, sTGFβR2 + αKlotho. *P < 0.01 compared with AAV:GFP-HFD; **P < 0.0001 values compared with AAV:GFP-HFD.

measured. Significant increases in both O_2 consumption and CO_2 production were observed, indicating a higher metabolic rate compared with the HFD AAV:GFP control mice (*SI Appendix,* Fig. S2). The respiratory exchange ratio (RER) was also found to shift from the dysregulation caused by the HFD, where lipids are the predominant fuel source, toward normal levels, where carbohydrates are principally metabolized (33, 34) (*SI Appendix,* Fig. S2*C*). Notably, the AAV:FGF21 mice did not display an increase in activity or a decrease in food consumption, strongly suggesting that the observed weight reduction was due solely to metabolic changes (*SI Appendix,* Fig. S2*C*). While we did not investigate to what extent fat absorption contributed to the phenotype (due to a decrease in bile production) (35), the marked changes in CO_2 and O_2 produced and consumed, respectively, suggest that it is largely due to metabolic effects. Computer-aided tomography (CT) and MRI were used to confirm that the mice given AAV:FGF21 (individually) did not lose bone or muscle mass compared with HFD controls, further confirming that weight loss was due to fat loss (Fig. 1 *F* and *G*).

Mice fed a prolonged HFD are also known to acquire a type II diabetes phenotype with poor glucose handling (36). Type II diabetes affects 30.3 million people and is a leading risk factor for heart diseases, kidney disease, and stroke (37). Therefore, to

investigate the effect of these therapies using a second disease model, a glucose tolerance test (GTT), an insulin tolerance test (ITT), a pyruvate tolerance test (PTT), and fasting blood glucose measurements were performed. GTT is used to assess how quickly an oral bolus of glucose can be cleared from the blood, ITT is used to evaluate the sensitivity of the animals to insulin, and PTT is used to ascertain the ability of the liver to produce glucose. Results of these assays showed that the AAV:FGF21 therapy alone completely mitigated the diabetic phenotype to varying degrees in combination with AAV:αKlotho and/or AAV:sTGFβR2, displaying an enhanced glucose response and recovered insulin sensitivity comparable with that of ND mice without affecting glucose production in the liver (Fig. 2 and *SI Appendix*, Fig. S3 *A* and *B*). While there are trending differences in the GTT curve for therapies AAV:αKlotho and AAV:sTGFβR2 individually or in combination, none are statistically significant without AAV:FGF21. The homeostatic model assessment for insulin resistance (HOMA-IR) and the homeostatic model assessment for β-cell function (HOMA-β) use combined fasting glucose and insulin levels to assess the overall function of this endocrine system. On testing, HOMA-IR showed improved function in HFD mice following treatment with all therapies and combinations compared with HFD AAV:GFP controls (Fig. 2 *E* and *F*). Interestingly, we saw a similar trend in the ability of the non-FGF21 therapies to improve insulin–glucose handling in the HOMA-IR and weight loss in old ND mice (Figs. 1*E* and 2*E*), suggesting that the HFD may "overpower" the weight loss effects of some of these therapies. However, the HFD was not able to completely abrogate the therapies' effect on this endocrine system as seen in the HOMA-IR. All 3 therapies provided a substantial and lasting effect following a single administration as opposed to administering them as biologics, whereupon the observed effect is temporary due to its short half-life (i.e., FGF21) (38).

Kidney failure and renal fibrosis are a major concern regarding the aging population in the United States, with more than 661,000 people either on dialysis or recipients of a kidney transplant (39). Over 38% of patients who experience kidney failure, in fact, eventually die from a cardiac event (39). αKlotho and TGFβ1 have been shown to be key factors in the progression of kidney failure in mice, and FGF21 has been shown to protect against chemotherapeutic kidney damage (18, 40–43). The third disease model used to evaluate the single and combination therapies used unilateral ureteral obstruction (UUO), an established means of simulating progressive renal fibrosis, which is a feature of renal disease (44). We injected mice with single and combination gene therapies 1 wk prior to disease induction via UUO, and kidneys were harvested and analyzed for fibrosis and remodeling 1 wk after the UUO procedure. Whole-kidney images stained with Masson's Trichrome stain (MTS) showed that overexpression of αKlotho was able to prevent deterioration of the renal medulla and thinning of the renal cortex compared with controls (Fig. 3 *A* and *B*). Surprisingly, the largest mitigation of medullary atrophy was due to the combination AAV:sTGFβR2 and AAV:FGF21, which performed significantly better than AAV:αKlotho at preventing renal medullary atrophy, with only 6.4% atrophy compared with 22.5%, respectively (*P* < 0.05) (Fig. 3 *A* and *B*). While kidney sections obtained from mice displayed only a slight increase in fibrosis at 7 d postsurgery, this is in line with earlier findings (18) that reported a trending difference between αKlotho transgenic and wild-type mice at day 7 that became significant at day 14 (Fig. 3*A* and *SI Appendix*, Fig. S4*B*). Myofibroblasts are key mediators of extracellular matrix formation and express α-smooth muscle actin (αSMA) (45). We stained kidney sections for this marker and observed lower αSMA expression compared to UUO controls. The AAV:FGF21 + AAV:sTGFbR2 therapy group had the largest effect with a 59% (*P* < 0.001) reduction in αSMA staining (Fig. 3 *C* and *D*). Surprisingly, we found that the AAV:FGF21 seemed to have a greater effect on medullary atrophy and αSMA than

Fig. 2. Systemic AAV delivery of combination gene therapy reverses symptoms of diabetes for mice on an HFD. (*A*) GTT of mice fasted overnight for 8 h. Blood glucose measured at 0, 15, 30, 60, and 120 min after oral gavage of 50 mg of glucose. (*B*) Area under the curve (AUC) of the GTT. (*C*) ITT of mice fasted for 6 h. Blood glucose measured at 0, 15, 30, 60, and 120 min after subcutaneous injection of 0.5 IU/kg insulin. (*D*) AUC of the ITT. (*E*) HOMA-IR. (*F*) HOMA-β. (*G*) Fasting insulin measurements of mice fasted for 8 h overnight before GTT. *n* = 10 for AAV:GFP ND mice, and *n* = 12 for AAV:GFP and AAV:FGF21 HFD mice. Statistical tests in *B* and *D–G* are 1-way ANOVA. Error bars represent SEM. C, control; F, FGF21; K, αKlotho; T, sTGFβR2; TF, sTGFβR2 + FGF21; TFK, sTGFβR2 + FGF21 + αKlotho; TK, sTGFβR2 + αKlotho; FK, FGF21 + αKlotho. **P < 0.05 values compare HFD-fed control and therapy-treated mice; ***P < 0.01 values compare HFD-fed control and therapy-treated mice; *†*P* < 0.0001 values compare HFD-fed control and therapy-treated mice.

AAV:αKlotho or AAV:sTGFβR2. Also unpredictably, the 2 groups that contained both AAV:FGF21 + AAV:αKlotho were worse than combinations of AAV:sTGFβR2 + AAV: αKlotho or AAV:sTGFβR2 + AAV:FGF21.

Heart failure is responsible for 425,000 deaths per year in the United States, with a prevalence of over 5.8 million people (46). Ascending aortic constriction (AAC) was selected as the fourth and final disease model, because it is a well-established mouse simulation of heart failure that mimics age-related hypertrophy caused by systemic hypertension (47, 48). The central role of TGFβ1 in heart remodeling and wound response suggested that sTGFβR2 (a repressor of TGFβ1) expression in the form of an AAV gene therapy could mitigate the progression of heart failure (24). Transgenic mice overexpressing either αKlotho or FGF21 have also been shown to slow the progression of this disease (19, 49, 50). Six-month-old mice were injected with AAV:sTGFβR2, AAV:αKlotho + AAV:sTGFβR2, AAV:FGF21 + AAV:sTGFβR2, or all 3 therapies combined 1 wk prior to measuring baseline echocardiograms (ECHOs) and performing AAC surgeries. Although the baseline ECHO did not reveal any influence of these therapies on normal heart function (Fig. 4 *A* and *B*), the surgical survival rates were 77% for AAV:sTGFbR2-treated mice and 87% for AAV:sTGFbR2 + AAV:αKlotho compared with only 50% for control mice (*P* < 0.1). This result suggests that there may be an increase in stress resistance that merits further investigation in future studies. Blood flow rate was also used to assess the relative constriction between all groups' ECHOs were performed on mice

APPLIED BIOLOGICAL SCIENCES
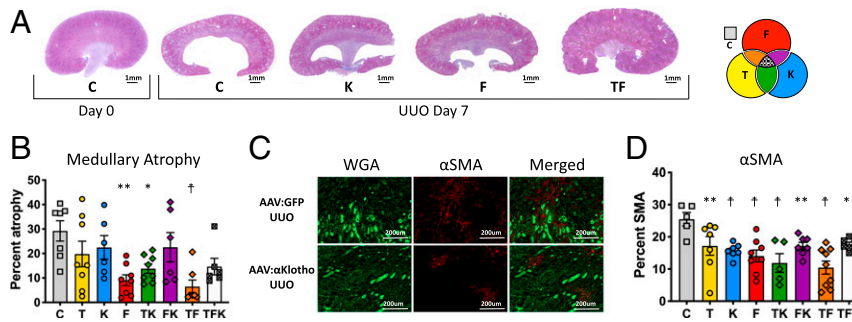
Fig. 3. Systemic AAV delivery of combination gene therapy mitigates renal damage due to UUO. (*A*) Representative MTS kidneys for mice that underwent UUO surgery at day 7 for control, AAV:αKlotho, AAV:FGF21, and AAV:FGF21 + AAV:sTGFbR2 therapy groups. (*B*) Quantification of renal medullary atrophy of different therapy group kidneys. Photoshop was used to calculate the area of atrophy by tracing inner and outer edges and measuring pixel area. If there was a discontinuity in the shape edge, an ellipse was used for approximation. *n* values are as follows: control (C) = 7, sTGFβR2 (T) = 8, αKlotho (K) = 6, FGF21 (F) = 8, TK = 8, FK = 6, TF = 7, TFK = 6. (*C*) Representative images of SMA- and WGA-stained kidneys. (*D*) Quantification of the ratio of SMA- to WGA-stained kidney sections. *n* values: C = 5, T = 7, K = 7, F = 8, TK = 5, FK = 7, TF = 9, TFK = 7. All images were taken at 10×, stitched together using Zen Zeiss software, and analyzed using custom MATLAB software that used color thresholding to separate different color pixels. Statistical tests in *B* and *D* are 1-way ANOVA. *P* values compare each therapy group with AAV:GFP. Error bars represent SEM. *P < 0.05; **P < 0.01; †*P* < 0.001. FK, FGF21 + αKlotho.

7, 30, and 90 d after surgery. At 90 d, the AAV:GFP control mice that had undergone AAC displayed a dilated phenotype with severe decreases in both contractility and output as measured by fractional shortening (FS) and ejection fraction (EF) (Fig. 4 *A–C*). We found that AAV:sTGFβR2 individually or combined with either AAV:FGF21 or AAV:αKlotho yielded an increased positive effect on heart function (Fig. 4 *A–C*). The seeming bimodality of the AAV:sTGFβR2 + AAV:αKlotho and AAV:sTGFβR2 + AAV:FGF21 groups suggests that there is a threshold amount of damage and preconditioning that can be rescued. In this way, we qualitatively observed a surprisingly worse outcome from the triple-therapy mixture compared with either the combination of AAV:sTGFβR2 + AAV:αKlotho or AAV:sTGFβR2 + AAV:FGF21 in that fewer mice were able to achieve wild-type EF and FS levels (Fig. 4 *A–C*). Mice that received AAV:sTGFβR2 + AAV:αKlotho experienced the largest gains, with a 222% increase in FS (i.e., 9.37 to 30.16; *P* < 0.002) and a 159% increase in EF (i.e., 20.91 to 54; *P* < 0.01) compared with AAV:GFP mice at 90 d (Fig. 4 *A–C*). Mouse hearts were collected and weighed after the final ECHO, and hearts from the 4 therapy-treated groups were found to be smaller (Fig. 4*D*). Body weight, organ weight, and tibia length were also recorded (*SI Appendix*, Table S1). We asked whether the increase in heart function observed in therapy-treated mouse groups was due to a reduction in remodeling and extracellular matrix formation as indicated by the increase in contractility and decrease in heart size. MTS sections revealed up to a 61% decrease in interstitial fibrosis (quantified by the amount of collagen deposition relative to normal heart tissue) on average for the combination therapy groups of AAV:STGFβR2 + AAV:FGF21 and AAV:STGFβR2 + AAV:αKlotho (Fig. 4 *E* and *F*), indicating a substantial mitigation of pathological progression despite the permanent restriction of blood flow.

Discussion

Beginning with the obesity model, we tested multiple therapeutic combinations and found that AAV:FGF21 together with either 1 or both of the other 2 gene therapies was able to mitigate the obesity phenotype in the HFD model as well as the aged ND model, although with a slightly diminished (nonsignificant) effect (Fig. 1). Proceeding to the type II diabetes model, we observed that all therapeutic combinations that included AAV:FGF21 rescued the HOMA-IR levels in the treated HFD mice (Fig. 2). Next, we applied the individual therapies and their combinations to the UUO model and found that all therapies elicited a positive effect on medullary deterioration and αSMA compared with control mice

(Fig. 3). Finally, the therapies were applied to the AAC heart failure model and corroborated the results from the other 3 models, with the largest effect observed for the combinations of AAV:sTGFβR2 with either AAV:FGF21 or AAV:αKlotho. Collectively, these data show that a single-combination therapeutic treatment consisting of AAV:sTGFβR2 and AAV:FGF21 can successfully treat all 4 age-related diseases at once. This combination had a higher therapeutic effect in both renal and heart failure compared with the individual gene therapies and maintained therapeutic effectiveness similar to the AAV:FGF21 therapy regarding obesity and diabetes, allowing for a better treatment overall for the 4 diseases involved in this study.

We initially hypothesized that, when administered as a single combination treatment, the AAV gene therapies would provide positive or possibly, additive effects against the 4 tested diseases. Indeed, an increased therapeutic effect was observed for AAV:sTGFβR2 combined with AAV:FGF21 or AAV:αKlotho in the renal and heart failure models. However, we also found an unexpected negative interaction between AAV:FGF21 and AAV:αKlotho. These 2 gene therapies performed worse when combined compared with their individual results for all 4 diseases, especially with regard to renal and heart failure. It will be interesting to investigate the underlying mechanistic interactions that led to this outcome in future studies to better inform our understanding of the responsible signaling networks and help determine suitable gene combinations in future experiments.

Although considerable knowledge has been gained from transgenics-based studies involving longevity-associated genes, modulation of their expression and testing in nontransgenic animals has remained elusive, and this is a critical step toward utilizing these mechanisms for the ultimate treatment of age-related conditions in humans. In this study, we have developed and tested individually and in combination 3 AAV-based gene therapies that express longevity-associated genes. Our approach attempts to increase the overall wellbeing of the individual by eliciting a widespread effect, mitigating multiple disease states at once, compared with traditional therapeutics that narrowly perturb a particular single gene/pathway (51). Importantly, this strategy also presents a more attractive path toward FDA approval by focusing on the treatment of age-related diseases, which have defined quantitative end points, whereas measuring an increase in longevity would require a lengthy (>20 y) and expensive clinical trial. The safety and health benefits of the expressed genes together with the low-risk profile of AAV-mediated gene delivery yield an approach that may avoid the risk of negative, off-target effects associated
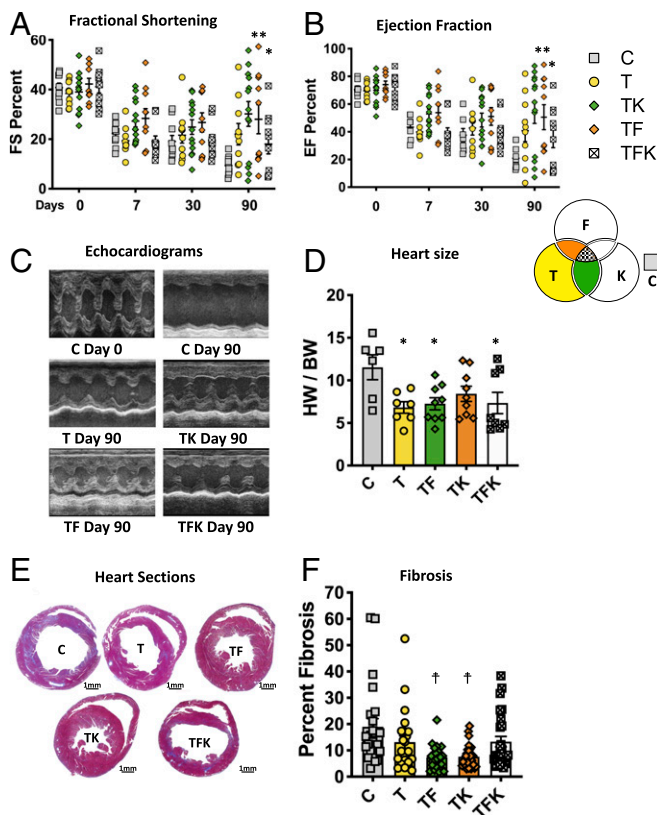
Fig. 4. Systemic AAV delivery of combination gene therapy stops progression of heart failure in an AAC mouse model. (*A*) FS quantification of ECHOs at baseline and 7, 30, and 90 d postsurgery. *n* = 10 for control (C), sTGFβR2 (T), sTGFβR2 + FGF21 (TF), and sTGFβR2 + FGF21 + αKlotho (TFK). *n* = 13 for sTGFβR2 + αKlotho (TK). (*B*) Representative ECHOs of mice at 3 mo post-AAC surgery. (*C*) Quantification of EF from ECHO. (*D*) Heart weight (HW) relative to body weight (BW) measured on day 90 post mortem. *n* for C = 6, *n* for T = 7, *n* for TF = 9, *n* for TK = 9, and *n* for TFK = 8. (*E*) Representative image of MTS hearts taken at 10× and stitched together. (*F*) Quantification of MTS-stained hearts. *n* for C = 10, *n* for T = 10, *n* for TF = 10, *n* for TK = 13, and *n* for TFK = 10. All images were taken at 10×, stitched together using Zen Zeiss software, and analyzed using custom MATLAB software that used color thresholding to separate different color pixels. Full ECHO data, including wall thickness, can be found in *SI Appendix*. Statistical tests in *A* and *B* are 2-way ANOVA, with *P* values representing comparison with AAV:GFP control mice over time. Statistical tests in *D* and *F* are 1-way ANOVA. Error bars represent SEM. F, FGF21. *P < 0.05; **P < 0.005; †P < 0.0002.

with small molecule therapies. While we have used the expression of 3 secreted factors as a proof of concept to avoid issues related to the codelivery of cell-autonomous factors (such as telomerase [12]), we believe that, as AAV capsids are continually engineered to enhance their infectivity, more cell-autonomous genes may be successfully used in combination in order to achieve similar if not improved results. Crucially, we have also demonstrated that individual longevity gene therapies can be easily combined into a single therapeutic mixture. This serves as an alternative to the traditional therapeutic approaches that, when concurrently treating multiple diseases, require multiple interventions with unrelated substances, which in turn, increase the accumulative exposure to negative side effects. A single-dose combination AAV therapy may also help alleviate issues associated with immune response when considering the alternative of multiple independent AAV-delivered therapies. Future studies may build on the combination AAV therapy concept presented here to treat the many diseases of aging and perhaps, also as a means to address the process of aging itself.

Methods

Vector Construction. The AAV plasmids were constructed by standard cloning techniques; full sequences of the genes can be found in *SI Appendix*. Briefly, the mouse versions of the genes FGF21, αKlotho, and sTGFβR2-fragment constant (FC) were PCR amplified using primers as follows: FGF21-Fwd-5′-cctgaa**cacctgcaacg**ggcctgccaccATGGAATGGATGAGATCTA-GAGTTGGGACC-3′ (the uppercase indicates the overlap to the FGF21 gene, and the bold indicates the AarI recognition site that creates an NotI overhang underlined), FGF21-Rev-5′-cctgaacgtctc**gctagc**ttaTCAGGACGCATAGCTGGGGC-3′ (the uppercase indicates the overlap to FGF21, and the bold indicates the NheI recognition site), αKlotho-fwd-5′-cctgaa**cacctgcaacg**ggcctgccaccATGCTA-GCCCGCGCCCCTCC, αKlotho-rev-cctgaacgtctc**gctagc**ttaTTACTTATAACT-TCTCTGGCC, sTGFbR2-fwd-5′-cctgaa**cacctgcaacg**ggcctgccaccATGGGTCGGG GGCTGCTCCGG-3′ (the uppercase indicates the overlap to the secretion signal of transforming growth factor-β receptor 2 [TGFβR2] receptor, and the bold indicates the AarI recognition site that creates an NotI overhang), sTGFbR2-Rev-5′-ggcttgattgtgggccctctggg GTCGGGACTGCTGGTGGTGTATTC-3′ (the bold indicates the overlap to the extracellular domain of TGFβR2 receptor, and the lowercase matches the igg2a sequence used for overlap PCR), Igg2a-Fwd-5′-gaatacaccaccagcagtcccgacCCCAGAGGGCCCACAATCAA-GCC-3′ (the bold indicates the overlap to the mouse Igg2a FC region, and the lowercase matches the extracellular domain of TGFβR2 sequence used for overlap PCR), and Igg2a-Rev 5′-cctgaa**cacctgcctta**ctagcTCATTTACCCGGAGTC-CGGGAGAAG-3′ (the bold indicates the AarI recognition site that creates an NheI overhang).

The National Center for Biotechnology Information (NCBI) accession numbers for FGF21, αKlotho, and TGFβR2 are 56636, 16591, and 21813, respectively.

Virus Production. The AAV was created using triple transfection of HEK293T cells and iodixanol gradient purification as described previously. Briefly, HEK293T cells were transfected using PEI max (1 mg/mL) at a 4:1 ratio to DNA. The helper plasmid, capsid, and gene of interest (inverted terminal repeat plasmid) were transfected at a 2:1:1 molar ratio. The media and cells were collected 72 h posttransfection. The cells were lysed with 3× freeze–thaw, treated with benzonase for 45 min, centrifuged to remove cellular debris before combining with the media, and filtered through a 0.2-μm filter; 40% polyethylene glycol 8000 was added to a final concentration of 8%. The media-containing virus was stirred for 1 h at 4 °C and then, left overnight. The media were then spun at 3,000 × g for 20 min, and the supernatant was discarded. The precipitate was resuspended in 5 mL of 1× phosphate buffered saline (PBS) and underlaid with a iodixanol gradient (15, 25, 40, and 60%) in opti-seal tubes (BECKMAN COULTER). Then, it was ultracentrifuged at 250,000 × g for 1 h in BECKMAN COULTER VTi50. The 40% fraction was collected and washed 5 times with 1× PBS containing 0.001% PLURONIC F65 (SIGMA) and stored in 1× PBS with 5% sorbitol and 0.001% PLURONIC F65 at −80 °C.

qPCR, ELISA, Western Staining, and Immunostaining. Virus was titered using qPCR with TaqMan Fast Advanced Master Mix (Thermo Fisher Scientific) to a common 3′ region of all vectors in the WPRE3 (woodchuck Posttranscriptional Regulatory Element): forward primer: 5′-CTTCCCGTATGGCTTTCATTTT, reverse primer: 5′-GCCGTGGCAAGAACTAACCA, and probe: 5′-FAM-TCCTCCTT-ZEN-GTATAAATC-IBFQ (IDT custom probe). ELISAs were performed for mouse TGFb1 and mouse FGF21 (ABCAM ab119557; ab212160). The antibody used for αKlotho is AF1819 from R&D SYSTEMS. αSMA was stained using ab5694 from ABCAM. Wheat germ agglutinin (WGA) was from ABCAM 20528, and DAPI was from SIGMA. Samples were formalin fixed for 24 h and then, paraffin embedded.

Mice. C57BL/6J male mice were purchased from Jackson Laboratories at the age indicated in the study. The mice were ear notched and tagged for identification, and then, they were housed in individually and positively ventilated polysulfonate cages with high-efficiency particulate air–filtered air at a density of 5 mice per cage. The animals were in Harvard Association for Assessment and Accreditation of Laboratory Animal Care (AAALAC)-accredited facilities. The animal room was lighted entirely with artificial fluorescent lighting, with a controlled 12-h light–dark cycle (7 AM to 7 PM light). Filtered tap water, acidified to a pH of 2.5 to 3.0, and normal rodent chow were provided ad libitum. For the UUO experiments, mice were purchased at 8 wk old (JAX stock 000664). For the obesity and diabetes experiments, mice were purchased at 17 wk old (JAX stock 380050). The mice used in the obesity study were immediately put on a 45% HFD D12451 (Research Diets Inc.) for the entire study. For the heart failure experiments, the mice were purchased at 26 wk of age (JAX stock 000664 at 30 ± 3 g). All mouse protocols were approved by the Harvard Institutional Animal Care and Use

Committee (IACUC) and Committee on Biological Safety (COMS) committees. The AAV was delivered via retroorbital injections. αKlotho and sTGFβR2 were each dosed at 1E11 vg per mouse, and FGF21 was dosed at 1E10 vg per mouse. All mice were randomized based on weight for each experiment.

OGTT, ITT, and PTT. All mice had been given an AAV therapy or control virus ~30 d before testing these parameters and had been on an HFD for ~4 to 5 mo. The mice were fasted overnight for 8 h for the oral glucose tolerance test (OGTT) and the pyruvate tolerance test (PTT). The mice were only fasted for 6 h for the insulin tolerance test (ITT). These were performed as previously described. Briefly, after fasting, the baseline blood glucose was measured; an oral bolus of 500 mg glucose was delivered for the OGTT, a 2-g/kg dose of pyruvate was administered intraperitoneally, or a 0.5-IU/kg dose of insulin was administered intraperitoneally. The blood glucose was measured at 15-, 30-, 60-, and 120-min intervals. The mice that were on an ND were given a 1-IU/kg dose of insulin. On seeing all of the FGF21 mice's blood glucose crash below 40 mg/dL after 30 min, the rest of the HFD mice were given a lower dose of 0.5 IU/kg. A One Touch Ultra glucose monitor and black strips were used.

UUO. Mice were placed on temperature-controlled heating pads maintained at 37 °C. Mice were positioned with the head and neck fully extended to ensure a patent airway. The temperature of the mice and the thermal pads were controlled at 37 °C via a rectal probe that monitors body temperature for the duration of the procedure. UUO was achieved by exposing the left kidney through the left flank. The ureter was obstructed completely near the renal pelvis using a 4-0 silk braided polyester Ethibond tie at 2 points. The skin was stapled using sterile staples. No sutures were used. The mice were then euthanized at 7 or 14 d postsurgery, and tissues and blood were collected for analysis. The mice were randomized and blinded from the surgeons such that they did not know which mice received which therapy.

AAC. Aortic constriction was induced in adult mice through constriction of ascending aorta. An incision was made in the chest wall at the third intercostal space. A rodent rib spreader was inserted, and the ribs were gently spread to allow access to the thoracic cavity. The ascending aorta was then isolated from the pulmonary artery, and a sterile 8-0 Prolene ligature was passed around it ~3 mm from the base of the heart. A blunted 26-gauge needle was placed on top of the aorta, and ligation was tied around the needle. The needle was then carefully removed from under the tie. The rib spreader was then removed, and the lung was reinflated. The ribs, chest musculature, and skin were closed using sterile 5.0 sutures (Vicryl and Prolene for closing muscle and subcutaneous layers and skin, respectively). Sham-operated animals underwent similar procedures without constriction of the aorta. Animals were closely monitored until full recovery from anesthesia. After the animal had regained consciousness (and was able to protect its airway), the animal was extubated. The surgeon minimized postoperative pneumothorax by placing the final thoracotomy rib-closing suture when the lungs were expanded. Animals were continually closely monitored until full neurological consciousness was achieved. Postoperatively, additional analgesic was administered for a minimum of 48 h. Animals were recovered on a heat source. The mice were randomized and blinded from the surgeons such that they did not know which mice received which therapy.

ECHOs. These were performed as previously described in "Transthoracic echocardiography in mice" by Respress and Wehrens (52). Briefly, mice were anesthetized and Naired. Then, preheated ultrasound gel was applied to the chest over the heart, and images were taken. The mice were randomized and blinded from the technicians such that they did not know which mice received which therapy.

Quantification of Images. Images of entire organs were taken at 10×, stitched together using Zen Zeiss software, and analyzed using custom MATLAB software. The MATLAB software used the color thresholding tool to first select the pixel colors of interest and then, to export this as code that can be used as a function call for all subsequent images. The script saved the pixel counts and exported them as a text file. The ratios were calculated by simply dividing the stain of interested vs. the total area of the organ. The total area of the organ was obtained by thresholding all colors vs. the background white surrounding the organ.

1. M. J. Divo, C. H. Martinez, D. M. Mannino, Ageing and the epidemiology of multimorbidity. *Eur. Respir. J.* **44**, 1055–1068 (2014).
2. K. Grumbach, Chronic illness, comorbidities, and the need for medical generalism. *Ann. Fam. Med.* **1**, 4–7 (2003).
3. C. Hajat, S. P. Kishore, The case for a global focus on multiple chronic conditions. *BMJ Glob. Health* **3**, e000874 (2018).
4. Y. Zhang *et al.*, The starvation hormone, fibroblast growth factor-21, extends lifespan in mice. *eLife* **1**, e00065 (2012).
5. H. Kurosu *et al.*, Suppression of aging in mice by the hormone Klotho. *Science* **309**, 1829–1833 (2005).
6. W. W. Brooks, C. H. Conrad, Myocardial fibrosis in transforming growth factor beta(1) heterozygous mice. *J. Mol. Cell. Cardiol.* **32**, 187–195 (2000).
7. J. P. de Magalhães, M. Stevens, D. Thornton, The business of anti-aging science. *Trends Biotechnol.* **35**, 1062–1073 (2017).
8. J. C. Newman *et al.*, Strategies and challenges in clinical trials targeting human aging. *J. Gerontol. A Biol. Sci. Med. Sci.* **71**, 1424–1434 (2016).
9. K. V. T. Engebretsen *et al.*, Attenuated development of cardiac fibrosis in left ventricular pressure overload by SM16, an orally active inhibitor of ALK5. *J. Mol. Cell. Cardiol.* **76**, 148–157 (2014).
10. J. Sonoda, M. Z. Chen, A. Baruch, FGF21-receptor agonists: An emerging therapeutic class for obesity-related diseases. *Horm. Mol. Biol. Clin. Investig.* **30**, /j/hmbci.2017.30. issue-2/hmbci-2017-0002/hmbci-2017-0002.xml (2017).
11. G. D. King *et al.*, Identification of novel small molecules that elevate Klotho expression. *Biochem. J.* **441**, 453–461 (2012).
12. B. Bernardes de Jesus *et al.*, Telomerase gene therapy in adult and old mice delays aging and increases longevity without increasing cancer. *EMBO Mol. Med.* **4**, 691–704 (2012).
13. A. Kharitonenkov *et al.*, FGF-21 as a novel metabolic regulator. *J. Clin. Invest.* **115**, 1627–1635 (2005).
14. M. Kuro-o *et al.*, Mutation of the mouse klotho gene leads to a syndrome resembling ageing. *Nature* **390**, 45–51 (1997).
15. M. C. Hu *et al.*, Renal production, uptake, and handling of circulating αKlotho. *J. Am. Soc. Nephrol.* **27**, 79–90 (2016).
16. D. Kajdaniuk, B. Marek, H. Borgiel-Marek, B. Kos-Kudła, Transforming growth factor β1 (TGFβ1) in physiology and pathology. *Endokrynol. Pol.* **64**, 384–396 (2013).
17. L. D. BonDurant *et al.*, FGF21 regulates metabolism through adipose-dependent and -independent mechanisms. *Cell Metab.* **25**, 935–944.e4 (2017).
18. M. Satoh *et al.*, Klotho protects against mouse renal fibrosis by inhibiting Wnt signaling. *Am. J. Physiol. Renal Physiol.* **303**, F1641–F1651 (2012).
19. J. Xie *et al.*, Cardioprotection by Klotho through downregulation of TRPC6 channels in the mouse heart. *Nat. Commun.* **3**, 1238 (2012).
20. S. Redondo, J. Navarro-Dorado, M. Ramajo, Ú. Medina, T. Tejerina, The complex regulation of TGF-β in cardiovascular disease. *Vasc. Health Risk Manag.* **8**, 533–539 (2012).
21. G. Buchlis *et al.*, Factor IX expression in skeletal muscle of a severe hemophilia B patient 10 years after AAV-mediated gene transfer. *Blood* **119**, 3038–3041 (2012).
22. L. A. George, Hemophilia gene therapy comes of age. *Blood Adv.* **1**, 2591–2599 (2017).
23. S. Daya, K. I. Berns, Gene therapy using adeno-associated virus vectors. *Clin. Microbiol. Rev.* **21**, 583–593 (2008).
24. H. Okada *et al.*, Postinfarction gene therapy against transforming growth factor-beta signal modulates infarct tissue dynamics and attenuates left ventricular remodeling and heart failure. *Circulation* **111**, 2430–2437 (2005).
25. C. Zincarelli, S. Soltys, G. Rengo, J. E. Rabinowitz, Analysis of AAV serotypes 1-9 mediated gene expression and tropism in mice after systemic injection. *Mol. Ther.* **16**, 1073–1080 (2008).
26. G. Schreiber, The synthesis and secretion of plasma proteins in the liver. *Pathology (Phila.)* **10**, 394 (1978).
27. National Institute of Diabetes and Digestive and Kidney Diseases (NIDDK), Overweight & obesity statistics. https://www.niddk.nih.gov/health-information/healthstatistics/overweight-obesity. Accessed 29 March 2018.
28. C. E. Wall *et al.*, High-fat diet and FGF21 cooperatively promote aerobic thermogenesis in mtDNA mutator mice. *Proc. Natl. Acad. Sci. U.S.A.* **112**, 8714–8719 (2015).
29. E. A. Forsberg, H. Olauson, T. Larsson, S. B. Catrina, Effect of systemically increasing human full-length Klotho on glucose metabolism in db/db mice. *Diabetes Res. Clin. Pract.* **113**, 208–210 (2016).
30. H. Yadav *et al.*, Protection from obesity and diabetes by blockade of TGF-β/Smad3 signaling. *Cell Metab.* **14**, 67–79 (2011).
31. F. Samad, K. Yamamoto, M. Pandey, D. J. Loskutoff, Elevated expression of transforming growth factor-beta in adipose tissue from obese mice. *Mol. Med.* **3**, 37–48 (1997).
32. J. Yan *et al.*, Obesity- and aging-induced excess of central transforming growth factor-β potentiates diabetic development via an RNA stress response. *Nat. Med.* **20**, 1001–1008 (2014).
33. P. M. Marvyn, R. M. Bradley, E. B. Mardian, K. A. Marks, R. E. Duncan, Data on oxygen consumption rate, respiratory exchange ratio, and movement in C57BL/6J female mice on the third day of consuming a high-fat diet. *Data Brief* **7**, 472–475 (2016).
34. Y. Nie, T. P. Gavin, S. Kuang, Measurement of resting energy metabolism in mice using oxymax open circuit indirect calorimeter. *Bio Protoc.* **5**, e1602 (2015).

35. M. M. Chen, C. Hale, S. Stanislaus, J. Xu, M. M. Véniant, FGF21 acts as a negative regulator of bile acid synthesis. *J. Endocrinol.* **237**, 139–152 (2018).

36. R. S. Surwit, C. M. Kuhn, C. Cochrane, J. A. McCubbin, M. N. Feinglos, Diet-induced type II diabetes in C57BL/6J mice. *Diabetes* **37**, 1163–1167 (1988).

37. National Institute of Diabetes and Digestive and Kidney Diseases (NIDDK), Diabetes statistics. https://www.niddk.nih.gov/health-information/health-statistics/diabetesstatistics. Accessed 29 March 2018.

38. R. Hecht *et al.*, Rationale-based engineering of a potent long-acting FGF21 analog for the treatment of type 2 diabetes. *PLoS One* **7**, e49345 (2012).

39. National Institute of Diabetes and Digestive and Kidney Diseases (NIDDK), Kidney disease statistics for the United States. https://www.niddk.nih.gov/health-information/health-statistics/kidney-disease. Accessed 29 March 2018.

40. F. Li, Z. Liu, C. Tang, J. Cai, Z. Dong, FGF21 is induced in cisplatin nephrotoxicity to protect against kidney tubular cell injury. *FASEB J.* **32**, 3423–3433 (2018).

41. S. Anuwatmatee, S. Tang, B. J. Wu, K.-A. Rye, K. L. Ong, Fibroblast growth factor 21 in chronic kidney disease. *Clin. Chim. Acta* **489**, 196–202 (2019).

42. S. Doi *et al.*, Klotho inhibits transforming growth factor-beta1 (TGF-beta1) signaling and suppresses renal fibrosis and cancer metastasis in mice. *J. Biol. Chem.* **286**, 8655–8665 (2011).

43. L.-J. Ma *et al.*, Transforming growth factor-beta-dependent and -independent pathways of induction of tubulointerstitial fibrosis in beta6(-/-) mice. *Am. J. Pathol.* **163**, 1261–1273 (2003).

44. R. L. Chevalier, M. S. Forbes, B. A. Thornhill, Ureteral obstruction as a model of renal interstitial fibrosis and obstructive nephropathy. *Kidney Int.* **75**, 1145–1152 (2009).

45. E. M. Zeisberg, S. E. Potenta, H. Sugimoto, M. Zeisberg, R. Kalluri, Fibroblasts in kidney fibrosis emerge via endothelial-to-mesenchymal transition. *J. Am. Soc. Nephrol.* **19**, 2282–2287 (2008).

46. A. L. Bui, T. B. Horwich, G. C. Fonarow, Epidemiology and risk profile of heart failure. *Nat. Rev. Cardiol.* **8**, 30–41 (2011).

47. A. C. deAlmeida, R. J. van Oort, X. H. T. Wehrens, Transverse aortic constriction in mice. *J. Vis. Exp.*, 1729 (2010).

48. A. Flemming, Cardiovascular disease: Rejuvenating the ageing heart. *Nat. Rev. Drug Discov.* **12**, 503 (2013).

49. Y. Joki *et al.*, FGF21 attenuates pathological myocardial remodeling following myocardial infarction through the adiponectin-dependent mechanism. *Biochem. Biophys. Res. Commun.* **459**, 124–130 (2015).

50. A. Planavila *et al.*, Fibroblast growth factor 21 protects against cardiac hypertrophy in mice. *Nat. Commun.* **4**, 2019 (2013).

51. D. J. Margul *et al.*, Reducing neuroinflammation by delivery of IL-10 encoding lentivirus from multiple-channel bridges. *Bioeng. Transl. Med.* **1**, 136–148 (2016).

52. J. L. Respress, X. H. T. Wehrens, Transthoracic echocardiography in mice. *J. Vis. Exp.* **39**, e1738 (2010).

APPLIED BIOLOGICAL SCIENCES